# A CLASS OF POLARIZATION-INVARIANT DIRECTIONAL CLOAKS BY CONCATENATION VIA TRANSFORMATION OPTICS

## J. Z. Li[1] and H. Y. Liu[2], *

[1]Shenzhen Institutes of Advanced Technology, Chinese Academy of Sciences, Shenzhen 518055, China

[2]Department of Mathematics and Statistics, University of North Carolina at Charlotte, Charlotte, NC 28223, USA

**Abstract**—This article is devoted to the construction and investigation of a class of polarization-invariant directional cloaks by concatenation of cloaking medium components via transformation optics. It improves the construction of the first polarization-invariant directional cloak, introduced by Agarwal et al. [1]. The main ingredient is to construct a capsuloid transformed metamaterial consisting of an $l^p$-cylindrical transformation map and two half $l^p$-spherical transformation maps. Numerical investigation is carried out to test the performances of the cloaks under different polarized incoming waves. A salient feature of our cloaks is compact-sizedness, namely the geometrical size is no longer dependent on the regularization parameter $\rho$ under the non-uniform map. In particular, we study the cloaking effect with respect to the regularization parameter $\rho$ and the incident direction.

## 1. INTRODUCTION

Two articles in *Science* in 2006 [11, 17] gave blueprints for making objects invisible to electromagnetic waves. Their ideas rely on transformation optics, one of several approaches used to design a cloak of invisibility. Transformation optics is based on the fundamental idea of the invariance of Maxwell's equations under simultaneous transformation of the domain and push-forward of the material properties. Before that, essentially the same idea was discovered by Greenleaf et al. in 2003 [9] in electrical impedance tomography (EIT).

Recently, significant progress has been achieved toward designing and constructing metamaterials that successfully cloak scatterers in assorted restricted circumstances, see, e.g., [3–8, 10, 13, 19–21] and references therein.

Directional cloaks, as opposed to full cloaks, have attracted much interest due to their promising real world applications. For instance, directional cloaks can be used to build invisible artillery/supply shelters that cannot be detected by reconnaissance aircrafts or drones that impinge waves almost vertically to the ground; In war time, collapsible invisible tunnels can be built for troop and tanks transportation when enemy's ground radar is known to be displaced in a fixed position.

Several polarization-selective directional (PSD) cloaks have been studied in [14, 15, 18]. Based on transformation optics, [14, 18] presented a diamond-shaped perfect cloak and an elliptic cylindrical one, respectively. Both cloaks rely on the fact that there is no scattering in the virtual space when an infinitesimally thin plane, with perfectly electric conducting (PEC) condition on both sides and parallel to the incident direction, is illuminated by the incident transverse magnetic (TM) wave with its polarization perpendicular to the surface. Using quasi-conformal mapping scheme developed in [11, 15] experimentally reported the promising performance of compact-sized directional carpet cloaks without the restriction of narrow bandwidth and high loss.

To circumvent the drawback of the dependence of the performance of PSD cloaks on the polarization of incoming electromagnetic waves, the first three-dimensional polarization-invariant directional (PID) cloak has been recently proposed in [1], motivated by the fact that there will be negligible scattering when the direction of the incident wave coincides with the axial direction of a very thin and elongated perfectly electric conducting (PEC) scatterer. The polarization-invariance of PID cloaks make them more desirable than PSD ones in real world applications.

However, the PID cloak suggested in [1] has a restriction of large size in the axial direction compared to the cloaked scatterer since the spatial transformation used to design the metamaterial cloaking medium is essentially isotropic (see [1, Eqs. (1) and (2)]). The performance of this cloaking device depends on the regularization parameter $\rho$, a measure of the thinness of the PEC scatterer in the virtual space. Isotropic transformation makes the resulting cloak very long in the axial direction compared with the other two in particular when a near-perfect directional cloak is desirable, namely $\rho$ is required to be very small. In this paper, we propose a new class of

three-dimensional PID cloaks via concatenation of cloaking medium components by transformation optics. It combines the advantages of compact-sized directional cloaks in [14, 15, 18] and the PID one in [1]. The main ingredient is to construct a capsuloid transformed metamaterial consisting of an $l^p$-cylindrical transformation map and two half $l^p$-spherical transformation maps. Numerical simulation is carried out to investigate the performances of the proposed cloaks.

## 2. DIRECTIONAL CLOAKING BY CONCATENATION

The key idea to construct a compact-sized polarization-invariant directional cloak is to attach to an $l^p$-cylinder of radius $r$ ($r = \rho$, $R_1$, $R_2$) and fixed length $L$

$$|y|^p + |z|^p = r^p, \quad \text{and} \quad -L/2 \le x \le L/2, \quad 1 \le p < \infty$$

$$\max(|y|, |z|) = r \quad \text{and} \quad -L/2 \le x \le L/2, \quad p = \infty$$

with two half $l^p$-spherical "caps" with radius $r$

$$|x \pm L/2|^p + |y|^p + |z|^p = r^p, \quad 1 \le p < \infty$$
$$\max(|x \pm L/2|, |y|, |z|) = r, \quad p = \infty$$

to produce a capsuloid directional cloak by concatenation. Fig. 1 depicts the geometrical shapes of $l^1$, $l^2$ and $l^\infty$ PID cloaks, respectively, which look likes Russian matryoshka dolls. The domain enclosed by the innermost and outermost boundaries in the virtual space are transformed to construct the metamaterial cloaking medium enclosed by the intermediate and outermost boundaries in the physical space.

In the sequel, we take the $l^\infty$-case as an example to demonstrate the construction of our new PID cloaks (see the bottom plot in Fig. 1). The other cases can be treated in a completely similar manner.
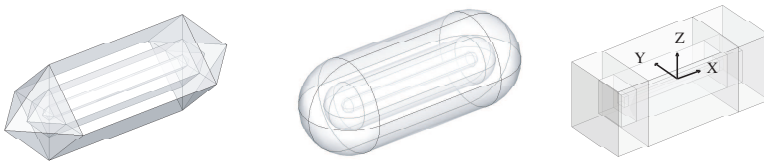


**Figure 1.** Directional cloaking devices depicted in both the virtual space (between innermost and outermost boundaries) and the physical space (between intermediate and outermost boundaries). From top to bottom: $l^1$-, $l^2$- and $l^\infty$-cloaks, respectively.

For the design of the $l^\infty$ PID cloak, we construct a special coordinate transformation from the virtual space $(x', y', z')$ to the physical space $(x, y, z)$. In the virtual space, a thin long $l^\infty$-cylinder with dimension $L \times 2\rho \times 2\rho$ is placed along the $x$-axis, with the center being at the origin. Concatenated on both thin tips of the $l^\infty$-cylinder are two half $l^\infty$-sphere with the dimension $\rho \times 2\rho \times 2\rho$. The surface of the concatenated $l^\infty$-capsuloid with dimension $(L + 2\rho) \times 2\rho \times 2\rho$ is PEC and the surrounding medium is free space.

As shown in Fig. 1, the to-be-transformed domain in the virtual space lying in between the innermost and outermost $l^\infty$-capsuloids with dimension $(L + 2\rho) \times 2\rho \times 2\rho$ and $(L + 2R_2) \times 2R_2 \times 2R_2$, respectively, is transformed to the cloaking medium in the physical space lying in between the $l^\infty$-capsuloids with dimension $(L + 2R_1) \times 2R_1 \times 2R_1$ and $(L + 2R_2) \times 2R_2 \times 2R_2$, respectively. As the counterpart of the PEC boundary of the innermost $l^\infty$-capsuloid in the virtual space, the intermediate boundary in the physical space is also PEC and scatterers can be cloaked within it. Note that $\rho < R_1 < R_2$ and $\rho \ll L$.

Moreover, the aforementioned cloaking medium in the physical space as well as its pre-image in the virtual space consists of six components, four quadrilateral frustums and two $l^\infty$-spherical caps resulting from the difference set of two $l^\infty$-concentric half-balls. The construction is divided into two steps by following notations of [1].

Firstly, for each to-be-transformed quadrilateral frustum in the virtual space, define $w$ to be the coordinate axis that is perpendicular to the inner and outer boundaries. The transform from the virtual space to the physical space for the $l^\infty$-cylinder is given by

$$\frac{y}{y'} = \frac{z}{z'}, \quad x = x' \tag{1}$$

$$\frac{w - w_i}{w' - w_i'} = \frac{w_o - w_i}{w_o - w_i'}, \tag{2}$$

where $w_i$ and $w_o$ are the coordinates of the inner and outer boundaries of the quadrilateral frustum and the counterparts are denoted in primed coordinates. Note that the outer boundaries in physical and virtual spaces are identical, $w_o' = w_o$. For later convenience, (2) can be written in a compact format,

$$w = w'K + Q, \tag{3}$$

where $K = \dfrac{w_o - w_i}{w_o - w_i'}$ and $Q = w_i - w_i'K$.

For example, in the upper quadrilateral frustum pointing along the $z$-axis, the $z$ axis is perpendicular to two boundaries, $w_i' = \rho$ and $w_o' = R_2$ in the virtual space, and $w_i = R_1$ and $w_o = w_o'$ in the physical

space. Thus, we have $w = z$ and the Jacobian matrix is given by

$$\bar{\bar{J}} = \begin{pmatrix} 1 & 0 & 0 \\ 0 & \dfrac{z}{z'} & -\dfrac{y'}{z'^2}Q \\ 0 & 0 & K \end{pmatrix}. \tag{4}$$

Thus, the relative permittivity and permeability tensors, $\bar{\bar{\epsilon}}/\epsilon_0$ and $\bar{\bar{\mu}}/\mu_0$, can be both calculated by following [17] to be

$$\bar{\bar{\epsilon}}_r = \bar{\bar{\mu}}_r = \frac{\bar{\bar{J}} \cdot \bar{\bar{J}}^{\mathrm{T}}}{\det \bar{\bar{J}}} = \begin{pmatrix} K^{-1}\dfrac{z'}{z} & 0 & 0 \\ 0 & K^{-1}\dfrac{z}{z'} + K^{-1}\dfrac{y'^2}{zz'^3}Q^2 & -\dfrac{y'}{zz'}Q \\ 0 & -\dfrac{y'}{zz'}Q & K\dfrac{z'}{z} \end{pmatrix}. \tag{5}$$

Secondly, for each to-be-transformed half $l^\infty$-spherical cap in the virtual space, define $w$ to be the coordinate axis that is along the $x$-axis with the origin displaced at $(\pm L/2, 0, 0)$, respectively. The transformation from the virtual space to the physical space for the half $l^\infty$-spherical cap is given by (2) and

$$\frac{x \pm L/2}{x' \pm L/2} = \frac{y}{y'} = \frac{z}{z'}, \tag{6}$$

where $w_i$ and $w_o$ in (2) should be now understood as the coordinates of the inner and outer boundaries of the half $l^\infty$-spherical cap but with the origin displaced at $(\pm L/2, 0, 0)$, respectively, and the counterparts are denoted in primed coordinates with the same displacement of the origin. Note that it still holds that $w'_o = w_o$ and (3) exists.

Thus, considering the left half $l^\infty$-spherical cap, we have $w = x + L/2$ as well as $w' = x' + L/2$ and the Jacobian matrix given by

$$\bar{\bar{J}} = \begin{pmatrix} K & 0 & 0 \\ -\dfrac{y'}{(x' + L/2)^2}Q & \dfrac{x + L/2}{x' + L/2} & 0 \\ -\dfrac{z'}{(x' + L/2)^2}Q & 0 & \dfrac{x + L/2}{x' + L/2} \end{pmatrix}. \tag{7}$$

Then, the relative permittivity and permeability tensors, $\bar{\bar{\epsilon}}_r = \bar{\bar{\epsilon}}/\epsilon_0 =$

$\bar{\bar{\mu}}_r = \bar{\bar{\mu}}/\mu_0 = \frac{\bar{\bar{J}} \cdot \bar{\bar{J}}^{\mathrm{T}}}{\det \bar{\bar{J}}}$, can be derived as follows:

$$
\bar{\bar{\epsilon}}_r = \begin{pmatrix}
K\dfrac{\left(x'+\frac{L}{2}\right)^2}{\left(x+\frac{L}{2}\right)^2} & -\dfrac{y'}{\left(x+\frac{L}{2}\right)^2}Q & -\dfrac{z'}{\left(x+\frac{L}{2}\right)^2}Q \\[4mm]
-\dfrac{y'}{\left(x+\frac{L}{2}\right)^2}Q & \dfrac{1}{K}+\dfrac{y'^2}{K\left(x+\frac{L}{2}\right)^2\left(x'+\frac{L}{2}\right)^2}Q^2 & \dfrac{y'z'}{K\left(x+\frac{L}{2}\right)^2\left(x'+\frac{L}{2}\right)^2}Q^2 \\[4mm]
-\dfrac{z'}{\left(x+\frac{L}{2}\right)^2}Q & \dfrac{y'z'}{K\left(x+\frac{L}{2}\right)^2\left(x'+\frac{L}{2}v\right)^2}Q^2 & \dfrac{1}{K}+\dfrac{y'^2}{K\left(x+\frac{L}{2}\right)^2\left(x'+\frac{L}{2}\right)^2}Q^2
\end{pmatrix}.
$$

$$(8)$$

The relative permittivity and permeability tensors in other three quadrilateral frustums and the right half $l^\infty$-spherical cap can be obtained similarly.

It is remarked that although the transformation from the virtual space to the physical space is defined subdomain-wise, it is not hard to see that the metamaterial parameters are smooth across the interface between two adjacent cloaking medium components. In turn, the invariance of Maxwell's equations under the proposed transformation still holds true. Therefore, the scattering behavior in the physical space is equal to that in the virtual space outside the cloaking medium. Due to the small scattering of thin wire when illuminated by the incoming wave along its axial direction with arbitrary polarization in the virtual space [2, 12], the scattering in the physical space would be also small when the same incident wave impinges upon the cloak.

## 3. NUMERICAL SIMULATIONS

In this section, we present the numerical simulations by employing the C++/Matlab coupled programming and the pardiso solver. Finite element method is used in a truncated spherical domain coated by a perfectly matched spherical layer to investigate the performance of the proposed cloaks. The far field pattern of the scattering field is calculated via the Stratton-Chu formula by surface integral on a sphere, within which the cloaking medium is compactly imbedded.

First of all, we study the scattering performance of the proposed cloaks. Three types of capsuloid cloaks with material parameters specified by (5) and (8) are illuminated by a $H_z$-polarized incident wave along the $x$-axis. For illustration, we plot the electromagnetic field distribution ($H_z$ component) and the Poynting energy flow on the $x$-$y$ plane. It can be seen from Fig. 2 that the electromagnetic
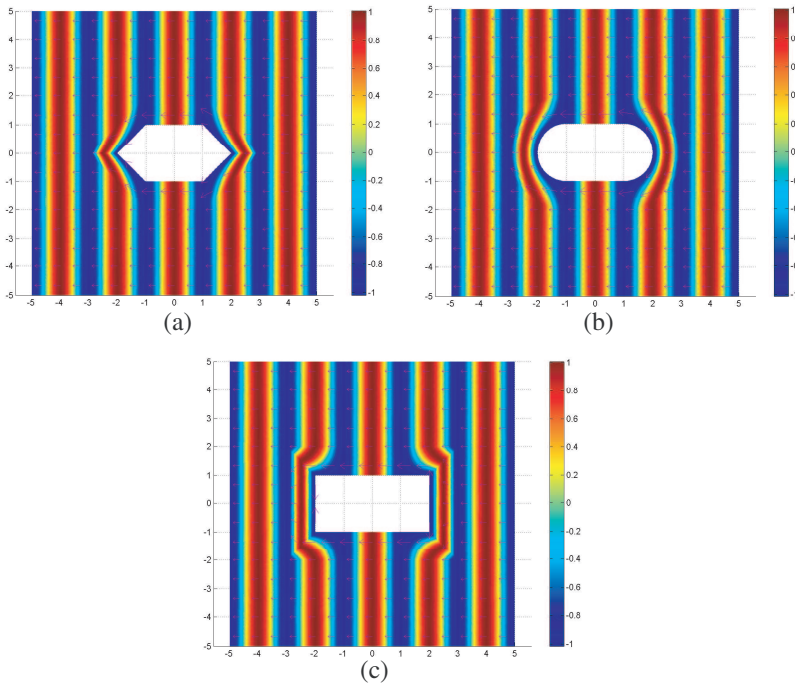
**Figure 2.** The slice plot of the $H_z$ field and the arrow plot of the electromagnetic Poynting power flow in the $x$-$y$ place. The $l^1$, $l^2$ and $l^\infty$ cloaks are all parametrized by $L = 1$, $\rho = 10^{-2}$, $R_1 = 1/2$, $R_2 = 1$, and illuminated by the $E_z$ polarized incident wave along the $x$-axis. (a) $l^1$ cloak. (b) $l^2$ cloak. (c) $l^\infty$ cloak.

wave and energy are guided around all three cloaks with negligible scattering. Similar scattering behavior can be observed when the polarization is perpendicular to the incident direction, which confirms the polarization-invariance of such directional cloaks.

Now we investigate the cloaking performance of the $l^\infty$-capsuloid cloak. Radar cross section (RCS), which is a measure of how detectable an object is and closely depends on the far field pattern of the scattering field, is adopted to measure the cloaking performance. Two RCSs (RCS$_\theta$ and RCS$_\phi$) are considered for the $\theta$ and $\phi$ components of the electric field, where $\theta$ and $\phi$ are respectively the inclination angle measured from the $z$-axis and the azimuthal angle in the spherical coordinate system. The scattered fields are measured in the $x$-$y$ plane ($\theta = \pi/2$). In the following, the RCSs are plotted in the polar diagram with the polar coordinates indicating the RCS strength in dB.
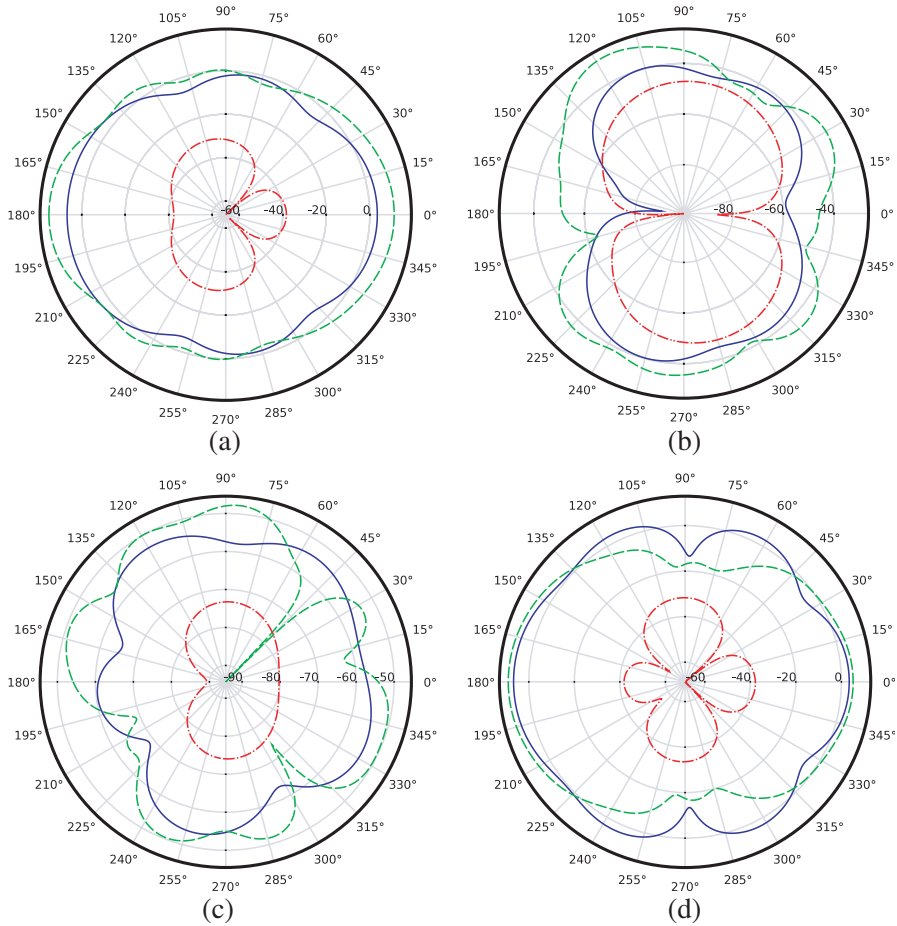
**Figure 3.** The RCSs for the $x$-axis incidence direction $(1, 0, 0)$ for bare PEC scatterer (green dashed line) and cloaked PEC scatterer with $\rho = 2^{-2}$ (blue solid line) and $\rho = 2^{-5}$ (red dash-dotted line) with $E_z$ (top) and $E_y$ (bottom) polarized incoming electric fields, respectively. (a) $\text{RCS}_\theta$ for $E_z$-polarized incidence. (b) $\text{RCS}_\phi$ for $E_z$-polarized incidence. (c) $\text{RCS}_\theta$ for $E_y$-polarized incidence. (d) $\text{RCS}_\phi$ for $E_y$-polarized incidence.

The following parameters are used in the following numerical simulations. The frequency $f$ of the incident EM wave is $300\,\text{MHz}$. The length of the cylinder $L = 1/2$. The radi of intermediate and outermost $l^\infty$-semi-spheres are $R_1 = 1/2$ and $R_2 = 1$, respectively. The regularization parameter $\rho$ ranges from $2^{-5}$ to $2^{-2}$. Thus, the

actual dimension of the capsuloid cloak is unchanged with length $5/2$.

First, we consider the incident wave with $E_z$ and $E_y$ polarizations, respectively, impinges along the ideal axial direction, i.e., the $x$-axis. Fig. 3 shows the RCS comparison of three cases: bare PEC scatter without cloak and cloaked PEC scatterer with the regularization parameter $\rho$ ranging from $2^{-2}$ to $2^{-5}$. In Fig. 3(a), we observe that the RCS$_\theta$ is more than $10\,\mathrm{dB}$ (green dashed line) for bare PEC scatterer, which is slightly decreased to about $5\,\mathrm{dB}$ (blue solid line) when relatively large regularization parameter ($\rho = 2^{-2}$) is used at 0 and 180 degrees. The corresponding RCS$_\theta$ for cloaked scatterer with $\rho$ being $2^{-5}$ is further reduced to be significantly small (below $-35\,\mathrm{dB}$, red dash-dotted line) for $E_z$ polarization in Fig. 3(a). Similar observation holds for RCS$_\phi$ in Fig. 3(d) for $E_y$ polarization. Figs. 3(b) and (c) show negligible scattering due to the orthogonality of the respective RCS component and the polarization. Consequently, by the linear superposition of the aforementioned two polarizations, the scattering from the cloaked PEC scatterer is comparably much smaller than that of the bare PEC one when $\rho$ is significantly decreased. The results are consistent with physical intuition since the scattering of the cloaked PEC capsuloid in the physical space is equivalent to that of a very thin and elongated PEC capsuloid embedded in air in the virtual space.

Next, we keep the same setting as above except changing the incident direction along the $y$-axis and test with $E_z$ and $E_x$ polarizations. It is highlighted that the incidence direction is perpendicular to the ideal direction (namely, the $x$-axis) in this case. We observe in Fig. 4(a) that the RCS$_\theta$ for bare PEC scatterer is obviously large (more than $15\,\mathrm{dB}$) in the forward and backward scattering region (green dashed line near the top and bottom regions). Furthermore, when the cloaking medium is employed and the regularization parameter is reduced from $2^{-2}$ to $2^{-5}$, Fig. 4(a) shows that $E_z$ polarization yields increasing cloaking effect, i.e., reducing RCS$_\theta$ from $10\,\mathrm{dB}$ (blue solid line) to below $-20\,\mathrm{dB}$ (red dash-dotted line) at 90 and 270 degrees. Meanwhile, Figs. 4(b) and (c) tell us that RCS$_\phi$ and RCS$_\theta$ are negligible due to their orthogonality to $E_z$ and $E_x$ polarizations, respectively.

On the other hand, we see from Fig. 4(d) that $E_x$ polarization gives poor cloaking effect by slightly reducing RCS$_\phi$ from $10\,\mathrm{dB}$ (blue solid line) to $-5\,\mathrm{dB}$ (red dash-dotted line) at 90 and 270 degrees, compared with $15\,\mathrm{dB}$ for bare PEC scatterer. This slow reduction of RCS$_\phi$ in Fig. 4(d), as opposed to the fast decay of RCS$_\theta$ in Fig. 4(a), can be explained by the theoretical expression of inductance of a wire, which is linearly dependent on the logarithm of the ratio of the wire's length

and thinness (or the regularization parameter $\rho$ here) [16]. As the regularization parameter $\rho$ gets smaller, the inductance of the thin wire increases but very slowly. Theoretically, the high inductance of the thin long PEC scatterer will render the proposed cloak invisible
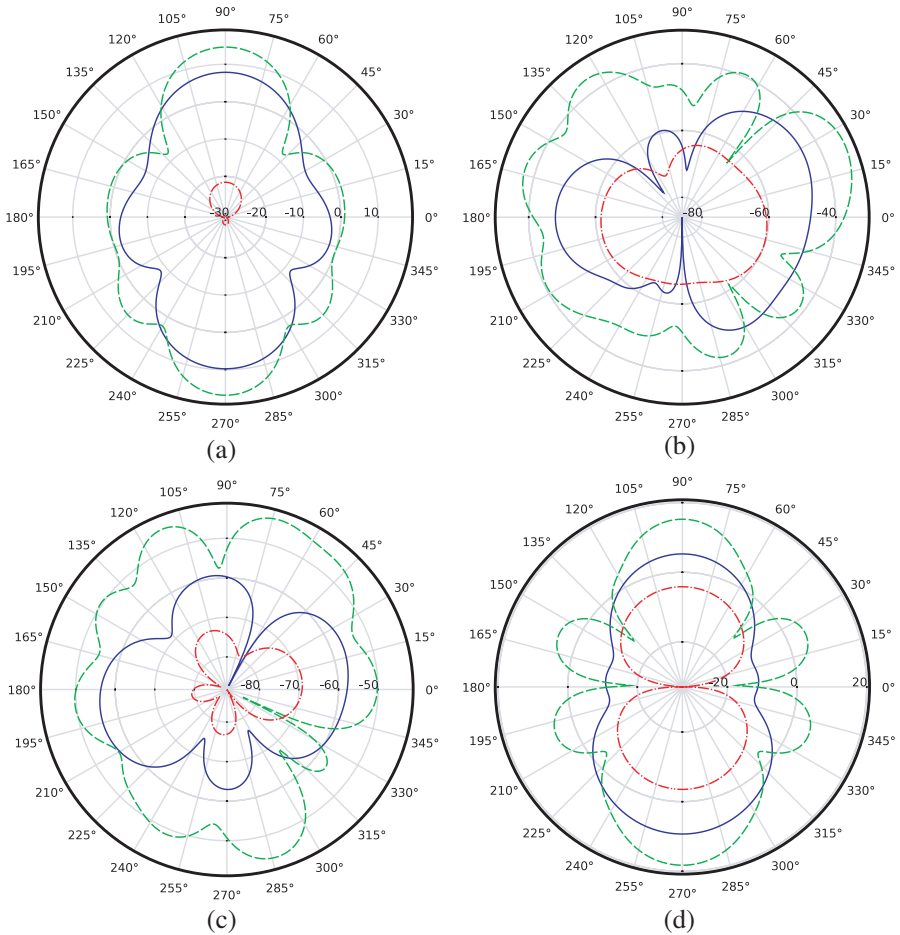


**Figure 4.** The RCSs for the $y$-axis incidence direction $(0, 1, 0)$ for bare PEC scatterer (green dashed line) and cloaked PEC scatterer with $\rho = 2^{-2}$ (blue solid line) and $\rho = 2^{-5}$ (red dash-dotted line) with $E_z$ (top) and $E_x$ (bottom) polarized incoming electric fields, respectively. (a) RCS$_\theta$ for $E_z$-polarized incidence. (b) RCS$_\phi$ for $E_z$-polarized incidence. (c) RCS$_\theta$ for $E_x$-polarized incidence. (d) RCS$_\phi$ for $E_x$-polarized incidence.

to radiation. Therefore the logarithmic increase of inductance with respect to $\rho$ makes the directional cloak illuminated by the $E_x$ polarized incident wave along the $y$-axis indeed performs but not so well for cloaking purpose. Another key observation in Fig. 4(d) is that $\mathrm{RCS}_\phi$ decays still fast at the two ends of the ideal direction ($x$-axis), namely from $-10\,\mathrm{dB}$ (blue solid line) to $-30\,\mathrm{dB}$ (red dash-dotted line) at 0 and 180 degrees when $\rho$ changes from $2^{-2}$ to $2^{-5}$. This directionally dependent fast decay can be explained by the reciprocal relation of the far field in the virtual space.

## 4. DISCUSSION AND CONCLUSION

We proposed a novel class of three-dimensional polarization-invariant directional cloaks, which is motivated by the negligibly small effect of a thin elongated PEC scatterer illuminated by the arbitrarily-polarized impinging wave along the axial direction. The proposed cloaks are numerically investigated. The cloaking performances can be properly controlled by the regularization parameter $\rho$ without elongating the cloaking devices. The new cloaking scheme could find important potential application in constructing compact-sized polarization-invariant directional cloaking devices.

## ACKNOWLEDGMENT

## REFERENCES

1. Agarwal, K., X. Cheng, L. Hu, H. Liu, and B.-I. Wu, "Polarization-invariant directional cloaking by transformation optics," *Progress In Electromagnetics Research*, Vol. 118, 415–423, 2011.

2. Bohren, C. F. and D. R. Huffman, *Absorption and Scatttering of Light by Small Particles*, Wiley, New York, 1983.

3. Chen, H., C. T. Chan, and P. Sheng, "Transformation optics and metamaterials," *Nature Materials*, Vol. 9, 387–396, 2010.

4. Chen, H., B. Zhang, Y. Luo, B. A. Kemp, J. Zhang, L. Ran, and B.-I. Wu, "Lorentz force and radiation pressure on a spherical cloak," *Phys. Rev. A*, Vol. 80, No. 1, 011808.1–011808.4, 2009.

5.  Cheng, X., H. Chen, X.-M. Zhang, B. Zhang, and B.-I. Wu, "Cloaking a perfectly conducting sphere with rotationally uniaxial nihility media in monostatic radar system," *Progress In Electromagnetics Research*, Vol. 100, 285–298, 2010.

6.  Cojocaru, E., "Illusion devices with internal or external circular objects designed by the coordinate transformation method," *Journal of Electromagnetic Waves and Applications*, Vol. 24, No. 16, 2309–2317, 2010.

7.  Greenleaf, A., Y. Kurylev, M. Lassas, and G. Uhlmann, "Improvement of cylindrical cloaking with the SHS lining," *Optics Express*, Vol. 15, No. 20, 12717–12734, 2007.

8.  Greenleaf, A., Y. Kurylev, M. Lassas, and G. Uhlmann, "Full-wave invisibility of active devices at all frequencies," *Communications in Mathematical Physics*, Vol. 275, 749–789, 2007.

9.  Greenleaf, A., M. Lassas, and G. Uhlmann, "Anisotropic conductivities that cannot be detected by EIT," *Physiological Measurement*, Vol. 24, 413–419, 2003.

10. Jiang, W. X., T. J. Cui, G. X. Yu, X. Q. Lin, Q. Cheng, and J. Y. Chin, "Arbitrarily elliptical-cylindrical invisible cloaking," *Journal of Physics D: Applied Physics*, Vol. 41, 085504, 2008.

11. Leonhardt, U., "Optical conformal mapping," *Science*, Vol. 312, 1777–1780, 2006.

12. Li, J. and J. B. Pendry, "Hiding under the carpet: A new strategy for cloaking," *Physical Review Letters*, Vol. 101, 203901, 2008.

13. Luo, Y., H. S. Chen, J. J. Zhang, L. X. Ran, and J. A. Kong, "Design and analytical full-wave validation of the invisibility cloaks, concentrators, and field rotators created with a general class of transformations," *Physical Review B*, Vol. 77, 125–127, 2008.

14. Luo, Y., J. J. Zhang, H. S. Chen, L. X. Ran, B. I. Wu, and J. A. Kong, "A rigorous analysis of plane-transformed invisibility cloaks," *IEEE Transactions on Antennas and Propagation*, Vol. 12, 3926–3933, 2009.

15. Ma, H. F., W. X. Jiang, X. M. Yang, X. Y. Zhou, and T. J. Cui, "Compact-sized and broadband carpet cloak and free-space cloak," *Optics Express*, Vol. 17, 19947–19959, 2009.

16. Rosa, E. B., "The self and mutual inductances of linear conductors," *Bulletin of the Bureau of Standards*, Vol. 4, No. 2, 301, 1908.

17. Pendry, J. B., D. Schurig, and D. R. Smith, "Controlling electromagnetic fields," *Science*, Vol. 312, 1780–1782, 2006.

18. Xi, S., H. S. Chen, B. I. Wu, and J. A. Kong, "One-directional perfect cloak created with homogeneous material," *IEEE Microwave and Wireless Components Letters*, Vol. 19, No. 3, 131–133, 2009.

19. Ye, D., S. Xi, H. Chen, J. Huangfu, and L.-X. Ran, "Achieving large effective aperture antenna with small volume based on coordinate transformation," *Progress In Electromagnetics Research*, Vol. 111, 407–418, 2011.

20. Zhai, Y.-B. and T.-J. Cui, "Three-dimensional axisymmetric invisibility cloaks with arbitrary shapes in layered-medium background," *Progress In Electromagnetic Research B*, Vol. 27, 151–163, 2011.

21. Zhang, B. L., H. S. Chen, B. I. Wu, and J. A. Kong, "Extraordinary surface voltage effect in the invisibility cloak with an active device inside," *Phys. Rev. Lett.*, Vol. 100, 063904, 2008.

22. Zhang, B. L., Y. Luo, X. G. Liu, and G. Barbastathis, "Macroscopic invisibility cloak for visible light," *Phys. Rev. Lett.*, Vol. 106, 033901, 2011.